RSC Advances

PAPER

View Article Online
View Journal | View Issue



Cite this: *RSC Adv.*, 2022, **12**, 35199

# Facile preparation of urchin-like $NiCo_2O_4$ microspheres for efficient hydrogen peroxide detection†

Jiaojiao Jiang, Zhixuan Zhang, Chong Yang, Rui Wang and Zhouling Wu *

Received 13th September 2022
Accepted 23rd November 2022

DOI: 10.1039/d2ra05778f

rsc.li/rsc-advances

In this work, urchin-like $NiCo_2O_4$ microspheres were prepared *via* a facile ionic liquid-assisted hydrothermal synthesis and used as non-enzymatic $H_2O_2$ sensors for the first time. The porous structure and high surface area of the $NiCo_2O_4$ microspheres provide plentiful active sites for electrocatalytic $H_2O_2$ oxidation. When adapted into an electrochemical sensor for $H_2O_2$, the microsensors showed fast response of 4 s, a high sensitivity of 392.5 $\mu A \cdot mM^{-1}$ $cm^{-2}$, and a wide linear range towards $H_2O_2$ (0–14 mM). The detection limit was as low as 0.05 μM, significantly lower than other published high performance $NiCo_2O_4$-based $H_2O_2$ sensors. Furthermore, this non-enzymatic sensor exhibits good selectivity for $H_2O_2$. These results suggest that $NiCo_2O_4$ microspheres could be a promising material for trace $H_2O_2$ detection.



## Introduction

$H_2O_2$ as a strong oxidant, has been widely used in the chemical industry, medical diagnosis, food safety and environmental analysis fields.[1–3] $H_2O_2$ also plays an important role in living organisms as a reactive oxygen species by driving oxidative biochemical processes and maintaining physiological redox homeostasis.[4] Excessive accumulation of $H_2O_2$ can cause many diseases, such as Alzheimer's disease, cardiovascular disorders, cancer, and Parkinson's.[5–8] Therefore, the development of $H_2O_2$ detection technologies is critical for disease-related diagnostics.

At present, $H_2O_2$ is typically detected using techniques such as fluorescence assays, chemiluminescence, and electrochemical method.[9–11] Among them, electrochemical method is considered one of the most promising method due to its low cost, fast response time, and high sensitivity.[12] Electrochemical sensors generally utilize enzymatic or non-enzymatic electrochemical materials for $H_2O_2$ detection.[13,14] Despite their high sensitivity and selectivity, enzymatic sensors can be expensive, sensitive to the surrounding environment (pH or temperature), and may have short lifespans, thus limiting their widespread practical applications.[14] Consequently, non-enzymatic sensors have received more attention as potential alternative methods.

In recent years, transition metal oxides have been widely used as electrochemical sensor nanomaterials for $H_2O_2$ detection. $NiCo_2O_4$ is a typical binary metal oxide, in which the coupling of Ni and Co ions provides the $NiCo_2O_4$ with greater electronic conductivity than either single-component $Co_3O_4$ and NiO materials, thereby enhancing the overall electrochemical performance of the nanomaterials.[15–17] Moreover, $NiCo_2O_4$ has high natural abundance, low cost and relatively low toxicity. Recently, research into $NiCo_2O_4$-based materials has mainly focused on the synthesis of various morphologies, such as nanoneedles, nanowalls, nanowires, nanorods, nanosheets, hollow structures and multilevel structures.[18–23] Among them, urchin-like structures have attracted extensive attention due to their high surface area, open structure and abundant active sites, all of which enhance the electrochemical performances of the nanomaterial.[23] However, reports on the preparation of urchin-like $NiCo_2O_4$ microspheres by an ionic liquid-assisted hydrothermal synthesis pathway has not been published.

Ionic liquids are often composed of hydrophobic organic cations and hydrophilic inorganic anions and can be an environmentally friendly green solvent, they are widely used as solvents and templates in the synthesis of nanomaterials.[24,25] In this work, urchin-like $NiCo_2O_4$ microspheres prepared *via* a facile ionic liquid-assisted hydrothermal synthesis are used as non-enzymatic $H_2O_2$ sensors for the first time. These $NiCo_2O_4$ microspheres exhibited excellent electrochemical properties and sensitivity towards $H_2O_2$ detection, demonstrating that the as-prepared hierarchical urchin-like $NiCo_2O_4$ microspheres could have potential applications as a non-enzymatic $H_2O_2$ sensor.

## Experimental

### Materials and reagents

$NiCl_2 \cdot 6H_2O$, $CoCl_2 \cdot 6H_2O$, urea ($CO(NH_2)_2$) and NaOH were provided by Tianjin Kemiou Chemical Reagent Co. Ltd. 1-Ethyl-

*School of Public Health, Zunyi Medical University, Zunyi 563000, Guizhou, P. R. China. E-mail: WuZhouLing90@163.com; Fax: +86 085128642732; Tel: +86 17385953536*

† Electronic supplementary information (ESI) available. See DOI: https://doi.org/10.1039/d2ra05778f

3-methylimidazolium nitrate ([EMIm]$NO_3$) was provided by Lanzhou Institute of Chemical Physics, CAS. $H_2O_2$ (30%, w/w) was supplied by Chongqing Wansheng Chuandong Chemical Co. Ltd. Nafion (5 wt% in ethanol) was provided by Aldrich. KCl, uric acid (UA), ascorbic acid (AA) and glucose were supplied by Aladdin Co. Ltd. All reagents were of analytical grade.

### Preparation of $NiCo_2O_4$

The $NiCo_2O_4$ microspheres were prepared using an ionic liquid-assisted hydrothermal method. First, 0.1 mol $L^{-1}$ $CoCl_2 \cdot 6H_2O$ and 0.05 mol $L^{-1}$ $NiCl_2 \cdot 6H_2O$ were dissolved in 20 mL deionized water. Second, 0.05 mol $L^{-1}$ 1-ethyl-3-methimidazole nitrate and 1.25 mol $L^{-1}$ urea was added and stirred for 0.5 h. Next, the mixture was transferred into a stainless steel autoclave and reacted at 100 °C for 10 h. Finally, the precipitates were collected by centrifugation, dried under overnight, and calcined in air at 400 °C for 2 h.

### Characterization

The morphology of products was observed using a Hitachi S-4800 Scanning electron microscopy (SEM) and ZEISS SUPRA 55 transmission electron microscopy (TEM). The annealing temperature was obtained in air by a thermogravimetric analyzer (PerkinElmer 6300). The phase structure of product was obtained using a Panalytical Empyrean X-ray diffraction spectrometer (XRD). X-ray photoelectron spectroscopy (XPS) was performed using a KRATOS AXIS ULTRA. The porosity and surface area were studied by $N_2$ adsorption (ASAP2460).

### Electrochemical measurements

Electrochemical experiments using a three-electrode system on CHI760E electrochemical workstation (Shanghai Chenhua Instrument Corporation, China) in 0.1 mol $L^{-1}$ NaOH solution. Pt mesh and Hg/HgO (1 mol $L^{-1}$ KCl) electrode were used as the counter electrode and reference electrode, for the fabrication of working electrode, a rotating-disk electrode (RDE, 5 mm) was polished with 0.03 μm $Al_2O_3$ slurry, followed by washing in sequence with aqueous nitric acid solution (1 : 3), water and ethanol. 2.0 mg of $NiCo_2O_4$ microspheres mixed with 50 μL Nafion was dispersed in 450 μL isopropanol aqueous solution (1 : 3 vol/vol isopropanol/water) and sonicated for 1 h. Finally, the well-dispersed ink (10 μL) was drop-casted onto the well-polished RDE surface, and then naturally dried to obtain working electrode ($NiCo_2O_4$/RDE). RDE rotation speed was 1600 rpm.

## Results and discussion

### Characterization of materials

To investigate the initial growth and formation mechanisms of the $NiCo_2O_4$ urchin-like microspheres, a detailed time course study was carried out. The synthetic reaction was monitored for up to 10 h, and scans of the related products at various time intervals (Fig. S1a–e†). After reacting for 2 h, a small number of nanowires clustered within the crystal nucleus into a broom shape (Fig. S1a†). Loose sea urchin-like structures gradually to form between 4–8 h (Fig. S1b–d†). When the reaction time was increased to 10 h, the urchin-like microspheres could eventually be obtained (Fig. S1e†). From this sequence, a possible formation mechanism is proposed as follows: first, the ionic liquids can exhibit easily aggregate and form micelles in solution.[25] After further adding urea into the $Ni^{2+}$ and $Co^{2+}$ containing water solution, the $OH^-$ anion slowly released during urea hydrolysis, then the metal cations ($Co^{2+}$ and $Ni^{2+}$) reacted with the $OH^-$ anion to form the $NiCo_2(OH)_6$ nucleus.[26] The large number of $NiCo_2(OH)_6$ nuclei were easily adsorbed on micellar surfaces of ionic liquid due to the low surface energy of ionic liquids. These nascent crystal nuclei further grow and self-assemble into nanorods, and eventually form the precursor of urchin-like $NiCo_2O_4$ microspheres. After calcination in air away the ionic liquid, the $NiCo_2(OH)_6$ are eventually decomposed into $NiCo_2O_4$ oxides, causing development of urchin-like $NiCo_2O_4$ hollow microspheres (Fig. 2e). Notably, in the absence of the ionic liquid [EMIm]$NO_3$, only $NiCo_2O_4$ solid microspheres were obtained by hydrothermal synthesis (Fig. S1f and g†). Therefore, the ionic liquid [EMIm]$NO_3$ is essential for the formation of the urchin-like microspheres. The relevant reactions are as follows:[26,27]

$$6CO(NH_2)_2 \rightarrow C_3N_6H_6 + 6NH_3 + 3CO_2 \quad (1)$$

$$NH_3 + H_2O \rightarrow NH_4^+ + OH^- \quad (2)$$

$$Ni^{2+} + 2Co^{2+} + 6OH^- \rightarrow NiCo_2(OH)_6 \quad (3)$$

$$2NiCo_2(OH)_6 + O_2 \rightarrow 2NiCo_2O_4 + 6H_2O \quad (4)$$

The optimal calcination temperature of the precursor was determined by thermogravimetric analysis (TG). According to the TG analysis (Fig. 1a), the 3.5 wt% loss below 200 °C due to dehydration. There was a significant reduction in wt% between 200 °C to 400 °C (22.2 wt%), indicating the decomposition of the precursor. Beyond 400 °C, the weight remains constant, indicating that the formation of a stable product. Therefore, the calcination temperature chosen for this study was 400 °C for 2 h.

The phase structures of the calcined product were obtained by XRD measurements (Fig. 1b). The XRD pattern exhibited six characteristic diffraction peaks at 18.9°, 31.1°, 36.7°, 44.6°, 59.1° and 64.9°. All these peaks can be attributed to the (111), (220), (311), (222), (511) and (440) crystal planes of $NiCo_2O_4$

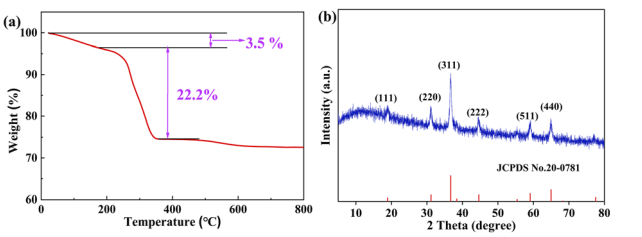


Fig. 1 (a) Thermogravimetric analysis of precursor. (b) XRD diagram of $NiCo_2O_4$.

(JCPDS No. 20-0781), indicating successful synthesis of $NiCo_2O_4$.

The morphologies of the products were obtained by SEM (Fig. 2). The precursor displays an urchin-like microsphere with a morphology of about 5 μm and consists of smooth nanowires (Fig. 2b). After calcination, the resulting $NiCo_2O_4$ maintains the same morphology as that of the precursor (Fig. 2c and e), but the $NiCo_2O_4$ microspheres are hollow structures and the nanowires of $NiCo_2O_4$ microspheres are composed of $NiCo_2O_4$ nanoparticles 25 nm in diameter (Fig. 2d and f). Meanwhile, the lattice images of HRTEM (Fig. 2g) showed *d*-spacing of 0.424, 0.208, 0.144 and 0.160 nm, corresponding to (111), (400), (440) and (422) crystal planes of $NiCo_2O_4$, respectively.

The porosity and surface area of $NiCo_2O_4$ microspheres were studied by $N_2$ adsorption and shown in Fig. 2h. A type IV isotherm was observed, confirming the a mesoporous structure of $NiCo_2O_4$ microspheres.[28] From this isotherm, the BET specific surface area was calculated as 52.15 $m^2\ g^{-1}$, and the average pore diameter and accumulative pore volume were calculated to be 17 nm and 0.21 $cm^3\ g^{-1}$, respectively. The high surface area and porous structure of $NiCo_2O_4$ should provide sufficient space for mass transfer, and also increase the available more active sites, both of which improve the electrocatalytic activity for $H_2O_2$ oxidation.

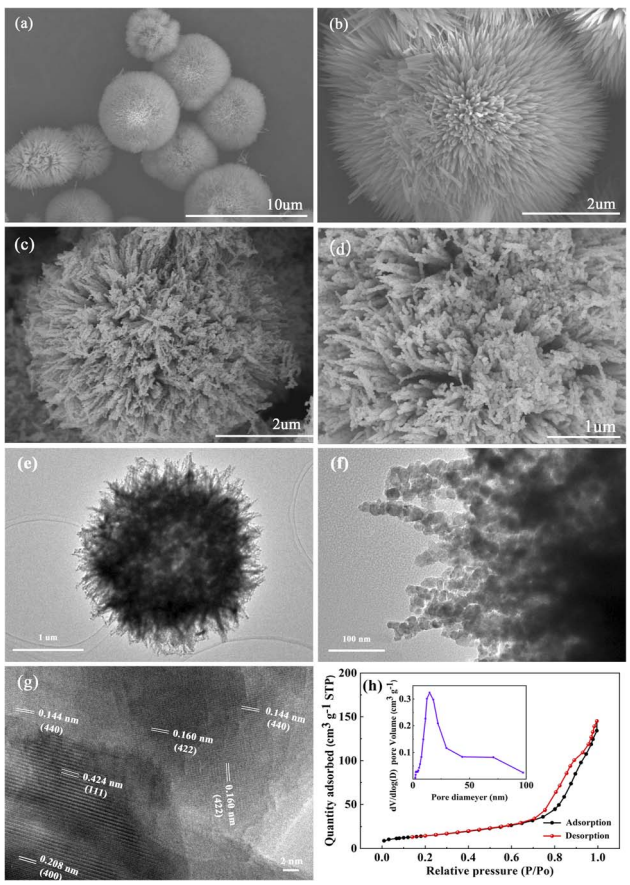


Fig. 2 SEM results of precursor (a and b) and $NiCo_2O_4$ (c and d). TEM (e and f) and HRTEM (g) image of $NiCo_2O_4$. (h) $N_2$ adsorption isotherm and the corresponding pore diameter distribution (inset) of $NiCo_2O_4$.

In order to confirm the surface chemical compositions of $NiCo_2O_4$ microspheres, we performed the XPS analysis (Fig. 3). The XPS full spectrum analysis (Fig. 3a) indicated only Ni, Co, O, and C in the $NiCo_2O_4$ microspheres. The Ni 2p spectra (Fig. 3b) shows two major peaks and two shakeup satellites (designated as "Sat."). The binding energies at 871.8 eV and 853.4 eV correspond to the Ni $2p_{1/2}$ and Ni $2p_{3/2}$, respectively. The Ni $2p_{1/2}$ and Ni $2p_{3/2}$ levels were best fitted with double peaks ($Ni^{2+}$ and $Ni^{3+}$) at high resolution. Similarly, the Co 2p spectra (Fig. 3c) shows the binding energy of Co $2p_{3/2}$ and Co $2p_{1/2}$ states at 779.1 eV and 794.2 eV, where the $Co^{3+}$ and $Co^{2+}$ valences are also clearly shown in the Co $2p_{3/2}$ and Co $2p_{1/2}$ levels. The presence of redox couples of $Ni^{3+}/Ni^{2+}$ and $Co^{3+}/Co^{2+}$ can significantly improve the electrocatalytic activity.[29] In addition, the O1s fine spectrum consists of three components (Fig. 3d). The binding energies of 529.1 eV, 530.6 eV and 532.3 eV were attributed to the lattice oxygen (designated as O1), oxygen withincrystalline defects (designated as O2) and physicochemically adsorbed oxygen (designated as O3), respectively.[30–32]

## Electrochemical properties of $NiCo_2O_4$/RDE

**Oxidation of $H_2O_2$ at the $NiCo_2O_4$/RDE.** The electrochemical properties of $NiCo_2O_4$ towards $H_2O_2$ oxidation were investigated by cyclic voltammetry (CV) and shown in Fig. 4a. The CV plot of $NiCo_2O_4$/RDE shows two pairs of redox peaks in the absence of $H_2O_2$, which correspond to the redox processes of $Co^{3+}/Co^{2+}$ and $Ni^{3+}/Ni^{2+}$ redox couples in the alkaline electrolyte.[33] Interestingly, upon addition of $H_2O_2$ into the NaOH electrolyte, the peak current of $NiCo_2O_4$/RDE increased significantly. This increased current correlated with increases in the $H_2O_2$ concentration (Fig. 4b). As a control, the CV obtained from a bare RDE is also shown in Fig. 4a.

The bare RDE only exhibited a weaker double-layer charging current, and does not show any redox peaks. These results suggested that the as-prepared $NiCo_2O_4$ microspheres are redox active and show electrocatalytic activity towards $H_2O_2$ oxidation. Furthermore, the CVs of $NiCo_2O_4$/RDE were studied at different scan rates (Fig. 4c). The anodic and cathodic peak currents

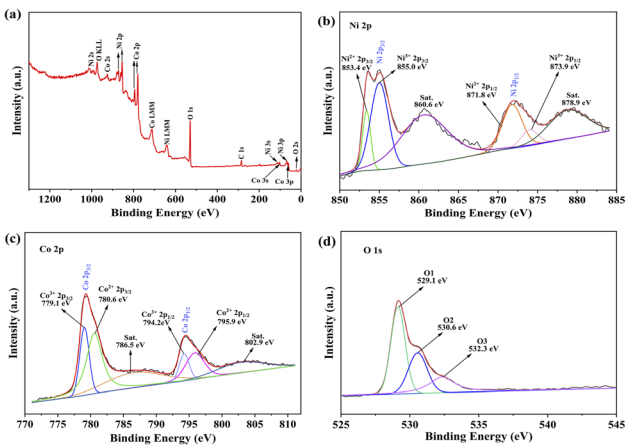


Fig. 3 XPS full spectrum (a), Ni 2p (b), Co 2p (c), and O 1s (d) for $NiCo_2O_4$.

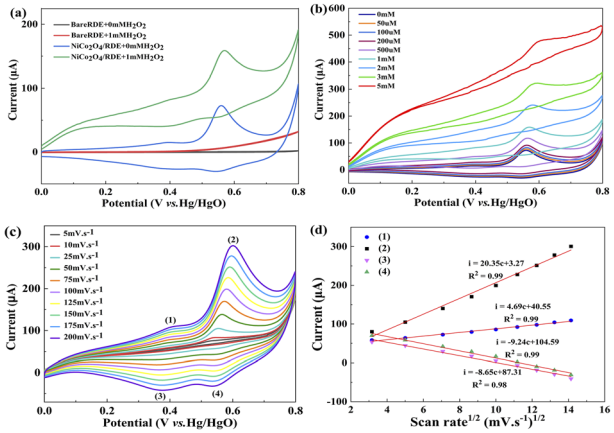


Fig. 4 (a) CVs of $NiCo_2O_4$/RDE with the absence and presence of 1 mM $H_2O_2$ in 0.1 M NaOH solution (scan rate 50 mV $s^{-1}$). (b) CVs of $NiCo_2O_4$/RDE with the addition of different amounts of $H_2O_2$ (scan rate 50 mV $s^{-1}$). (c) CVs of $NiCo_2O_4$/RDE at different scan rates with the presence of 1 mM $H_2O_2$. (d) The plot of cathodic and anodic peak currents *vs.* scan rates.

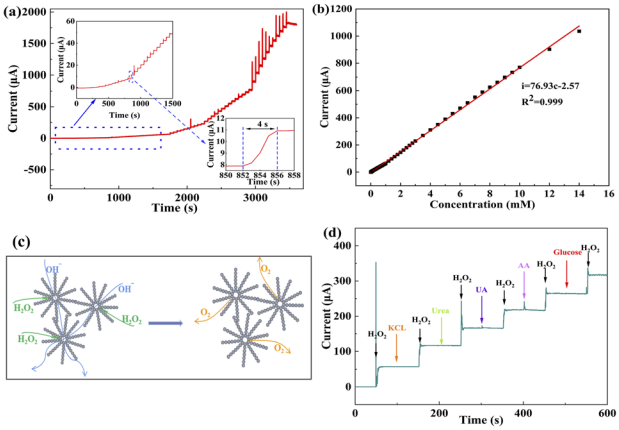


Fig. 5 (a) Amperometric response of $NiCo_2O_4$/RDE at 0.58 V and its corresponding calibration plot (b). (c) Schematic illustration of the oxidation process of $H_2O_2$ on the $NiCo_2O_4$. (d) Amperometric response of $NiCo_2O_4$/RDE in 0.1 M NaOH buffer following sequential addition of 1 mM $H_2O_2$, 0.1 mM KCL, 1 mM $H_2O_2$, 0.1 mM urea, 1 mM $H_2O_2$, 0.1 mM UA, 1 mM $H_2O_2$, 0.1 mM AA, 1 mM $H_2O_2$, 0.1 mM glucose.

increase with an increasing scanning rates, and the peak currents were directly proportional to the square root of scan rates (Fig. 4d). The above results suggested that the electrocatalytic/RDE was controlled by diffusion.[33] A possible catalytic mechanism involving $NiCo_2O_4$ is proposed as follows:[33]

$$NiCo_2O_4 + H_2O + OH^- \rightarrow 2CoOOH + NiOOH + e^- \quad (5)$$

$$2CoOOH + 3H_2O_2 \rightarrow 2Co(OH)_2 + 2H_2O + 2O_2 \quad (6)$$

$$2NiOOH + 3H_2O_2 \rightarrow 2Ni(OH)_2 + 2H_2O + 2O_2 \quad (7)$$

**Amperometric response of the $NiCo_2O_4$/RDE towards $H_2O_2$.** We investigated the effect of the applied potential and catalyst loading on the amperometric response of $NiCo_2O_4$/RDE towards $H_2O_2$ oxidation as shown in Fig. S2.† A potential of 0.58 V was selected as the optimal applied potential by comparing the noise current and sensitivity (Fig. S2a and b†). The sensitivity and linear range reached a maximum value when 200 μg $cm^{-2}$ $NiCo_2O_4$ was loaded onto the RDE (Fig. S2c and Table S1†). Therefore, this amount was used in the following studies.

The steady state amperometric response of $NiCo_2O_4$/RDE to successive additions of $H_2O_2$ at 0.58 V are shown in Fig. 5a. The $NiCo_2O_4$/RDE responded immediately following $H_2O_2$ addition, and the current stabilized within 4 s after adding $H_2O_2$ into the NaOH solution, suggesting that the $NiCo_2O_4$/RDE has a rapid and sensitive response behavior to $H_2O_2$. The response current was measured as a function of $H_2O_2$ concentration, which exhibited a linear response between 0 μM to 14 mM (Fig. 5b). The calculated sensitivity and detection limit of $H_2O_2$ from these measurements were 392.50 μA $mM^{-1}$ $cm^{-2}$ and 0.05 μM (S/N = 3), respectively. This marks a significant decreased in detection limit in comparison to previously reported $NiCo_2O_4$-based $H_2O_2$ nonenzymatic biosensors (Table 1). The rapid and sensitive response of the $NiCo_2O_4$ urchin-like microspheres was attributed to their unique hierarchical architecture, as shown in Fig. 5c. The $NiCo_2O_4$ urchin-like microsphere consists of nanowires and abundant pores, which not only are beneficial to the transport of $H_2O_2$ and electrolyte, but also allow the oxygen to rapidly escape from the surface of the catalyst, and the $H_2O_2$ and electrolyte to effectively infiltrate into the catalyst for continuing catalysis processes.

**Assessing the selectivity and stability of the $NiCo_2O_4$/RDE sensor for $H_2O_2$ detection.** To investigate the selectivity of the $NiCo_2O_4$/RDE sensor for $H_2O_2$ detection, the amperometric responses of $NiCo_2O_4$/RDE to $H_2O_2$ were studied in the presence of common biological interfering compounds, including KCl, urea, AA, UA and glucose (Fig. 5d). These results demonstrate that there is almost a negligible amperometric response towards all reagents except for $H_2O_2$, which shows a significant amperometric response. Therefore, the $NiCo_2O_4$ microspheres appear to be excellent selective for $H_2O_2$ detection. In order to assess the reproducibility of $NiCo_2O_4$/RDE as athe $H_2O_2$ sensor, five different $NiCo_2O_4$/RDE were independently fabricated by the same method. The amperometric responses of these electrodes to addition of 1 mM $H_2O_2$ were recorded. As a result, the relative standard deviation (RSD) of the response current was 5.4% ($n = 5$). The $NiCo_2O_4$/RDE sensor maintains 98.1% of its initial amperometric response upon addition of 1 mM $H_2O_2$ after storage in air for 15 days. For each individual sensor, the RSD in measured current response from fifteen successive measurments 0.43% ($n = 15$). Moreover, the stability of urchin-like morphology after the fifteen successive test was further checked by TEM and HRTEM analysis. The TEM image clearly show the urchin-like morphology, even after the fifteen successive test (Fig. S1h†). The lattice images of HRTEM (inset of Fig. S1h†) showed *d*-spacing of 0.246, 0.234 and 0.208 nm, corresponding to (311), (222) and (400) crystal planes of $NiCo_2O_4$, respectively. All these results suggest that the sensor

Table 1 The performance comparison of our proposed with other published for $H_2O_2$ sensors

| Material | Linear ranges (mM) | Detection limit (μM) | Ref. |
|---|---|---|---|
| $NiCo_2O_4$ | 0–14 | 0.05 | This work |
| NHGH/$NiCo_2O_4$ | 0.001–0.51 | 0.136 | 33 |
| ZnO/$Co_3O_4$/$NiCo_2O_4$/Ni foam | 0.0002–2.4 | 0.163 | 16 |
| $Co_3O_4$/NCNTs | 0.005–11 | 1 | 34 |
| $Co_3O_4$/$NiCo_2O_4$ | 0.05–41.7 | 0.2578 | 35 |
| NiO/$Ti_3C_2T_x$ | 0.01–4.54 | 0.348 | 36 |
| PbS/$Co_3O_4$ | 0.005–0.25 | 1.2 | 37 |
| $Ni_xCo_y$-DO | 0–0.4 | 0.28 | 38 |
| $NiCo_2O_4$/$CoNiO_2$@pRGO$_{600}$ | 0.005–3, 3–12 | 0.41 | 39 |
| NiO-MNS | 0.01–0.8 | 0.62 | 40 |
| Ni/NiO@C | 0.05–6.7, 8.7–80.7 | 0.9 | 41 |

had good reproducibility, repeatability and stability for the $H_2O_2$ detection.

## Conclusion

In conclusion, urchin-like $NiCo_2O_4$ microspheres were successfully fabricated *via* a relatively simple ionic liquid-assisted hydrothermal method and were used as an effective electrochemical sensor for $H_2O_2$. The results demonstrate that the urchin-like $NiCo_2O_4$ microspheres had structural properties that were ideal for its use as a non-enzymatic $H_2O_2$ sensor. The $H_2O_2$ sensor based on $NiCo_2O_4$ microspheres exhibited a fast detection response, a wide linear range, and high sensitivity towards $H_2O_2$. The high $H_2O_2$ detection performance achieved by $NiCo_2O_4$ in this study suggests these microspheres could have promising potential applications as $H_2O_2$ sensors in the medical diagnosics and biotechnology sectors.

## Author contributions

Jiaojiao Jiang: data curation, writing – original draft. Zhixuan Zhang: validation. Chong Yang: conceptualization, data curation. Rui Wang: methodology, data curation. Zhouling Wu: project administration, writing – review & editing.

## Conflicts of interest

There are no conflicts to declare.

## Acknowledgements

This work was supported by the Youth Program of National Natural Science Foundation of China (22102221), the Guizhou Provincial Natural Science Foundation (QKH-J[2019]1339 and QKH-J[2020]1Z006), and the projects of Zunyi Medical University (F-943).

## Notes and references

1 M. Asif, H. T Wang, D. Shuang, A. Aziz, G. A. Zhang, F. Xiao and H. F. Liu, Metal oxide intercalated layered double hydroxide nanosphere: with enhanced electrocatalytic activity towards $H_2O_2$ for biological application, *Sens. Actuators, B*, 2017, **239**, 243–252.
2 Y. Shu, B. Li, Q. Xu, P. Gu, X. Xiao, F. P. Liu, L. Y. Yu, H. Pang and X. Y. Hu, Cube-like $CoSn(OH)_6$ nanostructure for sensitive electrochemical detection of $H_2O_2$ in human serum sample, *Sens. Actuators, B*, 2017, **241**, 528–533.
3 B. Sherino, S. Mohamad, S. N. A. Halim and N. S. A. Manan, Electrochemical detection of hydrogen peroxide on a new microporous Ni-metal organic framework material-carbon paste electrode, *Sens. Actuators, B*, 2018, **254**, 1148–1156.
4 M. M. Liu, R. Liu and W. Chen, Graphene wrapped $Cu_2O$ nanocubes: Non-enzymatic electrochemical sensors for the detection of glucose and hydrogen peroxide with enhanced stability, *Biosens. Bioelectron.*, 2013, **25**, 206–212.
5 T. Shi, D. M. K. V. Soest, P. E. Polderman, B. M. T. Burgering and T. B. Dansen, DNA damage and oxidant stress activate p53 through differential upstream signaling pathways, *Free Radical Biol. Med.*, 2021, **172**, 298–311.
6 Y. J. Sun, M. C. Luo, Y. N. Qin, S. H. Zhu, Y. J. Li, N. Y. Xu, X. X. Meng, Q. S. Ren, L. Wang and S. J. Guo, Atomic-thick PtNi nanowires assembled on graphene for high-sensitivity extracellular hydrogen peroxide sensors, *ACS App. Mater. Interfaces*, 2017, **9**, 34715–34721.
7 F. Y. Xu, W. Tang, S. S. Kang, J. S. Song and X. R. Duan, A highly sensitive and photo-stable fluorescent probe for endogenous intracellular $H_2O_2$ imaging in live cancer cells, *Dyes Pigm.*, 2018, **153**, 61–66.
8 P. Cecilia, H. Silvana and D. Fiorentini, Peroxiporins in Cancer, *Int. J. Mol. Sci.*, 2019, **20**, 1371.
9 S. Duanghathaipornsuk, E. J. Farrell, A. C. Albarubio, P. Zelenay and D. S. Kim, Detection technologies for reactive oxygen species: fluorescence and electrochemical methods and their applications, *Biosensors*, 2021, **11**, 30.
10 B. Kalyanaraman, G. Cheng, M. Hardy, O. Ouari, B. Bennett and J. Zielonka, Teaching the basics of reactive oxygen species and their relevance to cancer biology: Mitochondrial reactive oxygen species detection, redox signaling, and targeted therapies, *Redox Biol.*, 2018, **15**, 347–362.

11 H. Cheng, Z. Y. Zhou and T. Liu, Electro-spinning fabrication of nitrogen, phosphorus co-doped porous carbon nanofiber as an electro-chemiluminescent sensor for the determination of cyproheptadine, *RSC Adv.*, 2020, **10**, 23091–23096.

12 E. Dumitrescu and S. Andreescu, Bioapplications of electrochemical sensors and biosensors, *Methods Enzymol.*, 2017, **589**, 301–350.

13 D. Thatikayala, D. Ponnamma, K. K. Sadasivuni, J. J. Cabibihan, A. K. Al-Ali, R. A. Malik and B. Min, Progress of Advanced Nanomaterials in the Non-Enzymatic Electrochemical Sensing of Glucose and $H_2O_2$, *Biosensors*, 2020, **10**(11), 151.

14 S. A. Hira, M. Nallal, K. Rajendran, S. Song, S. Park, J. M. Lee, S. H. Joo and K. H. Park, Ultrasensitive detection of hydrogen peroxide and dopamine using copolymer-grafted metal-organic framework based electrochemical sensor, *Anal. Chim. Acta*, 2020, **1118**, 26–35.

15 W. F. Liu, Z. H. Zhou, L. Yin, Y. M. Zhu, J. Zhao, B. Zhu, L. B. Zheng, Q. Jin and L. Wang, A novel self-powered bioelectrochemical sensor based on $CoMn_2O_4$ nanoparticle modified cathode for sensitive and rapid detection of hydrogen peroxide, *Sens. Actuators, B*, 2018, **271**, 247–255.

16 B. Xue, K. Z. Li, S. Y. Gu, L. L. Zhang and J. H. Lu, Ni foam-supported ZnO nanowires and $Co_3O_4$/$NiCo_2O_4$ double-shelled nanocages for efficient hydrogen peroxide detection, *Sens. Actuators, B*, 2018, **262**, 828–836.

17 R. Kumar, $NiCo_2O_4$ nano-microstructures as high-performance biosensors: a review, *Nano-Micro Lett.*, 2020, **12**, 2150–5551.

18 Q. Guo, W. Zeng and Y. Q. Li, Highly sensitive non-enzymatic glucose sensor based on porous $NiCo_2O_4$ nanowires grown on nickel foam, *Mater. Lett.*, 2019, **256**, 126603.

19 L. J. Liu, Z. H. Wang, J. H. Yang, G. L. Liu, J. J. Li, L. Guo, S. L. Chen and Q. H. Guo, $NiCo_2O_4$ nanoneedle-decorated electrospun carbon nanofiber nanohybrids for sensitive non-enzymatic glucose sensors, *Sens. Actuators, B*, 2018, **258**, 920–928.

20 Y. Ni, J. Xu, H. Liu and S. J. Shao, Fabrication of RGO-$NiCo_2O_4$ nanorods composite from deep eutectic solvents for nonenzymatic amperometric sensing of glucose, *Talanta*, 2018, **185**, 335–343.

21 X. M. Zhang, Y. X. Zhao, Y. T. Wu and Z. X. Mao, Two-dimensional hexagonal $NiCo_2O_4$ nanoplates@PEDOT/RGO nanocomposite: A design and construction high selective $H_2O_2$ sensing interface, *J. Electrochem. Soc.*, 2020, **167**, 067519.

22 Q. Chen, Y. H. Zhang, S. Y. Ma, Y. H. Wang, P. Y. Wang, G. H. Zhang, D. J. Gengzang, H. Y. Jiao, M. X. Wang and W. J. Chen, Multishelled NiO/$NiCo_2O_4$ hollow microspheres derived from bimetal-organic frameworks as high-performance sensing material for acetone detection, *J. Hazard. Mater.*, 2021, **415**, 125662.

23 M. Z. Khan, J. H. Zhu and X. H. Liu, Reduced graphene oxide-conjugated urchin-like $NiCo_2O_4$ nanostructures for individual detection of o-nitro and p-amino phenol, *ACS Omega*, 2019, **4**, 11433–11439.

24 L. J. Yang, Y. D. Hu, Q. Wang, Y. Y. Dong and L. Zhang, Ionic liquid-assisted electrochemical determination of pyrimethanil using reduced graphene oxide conjugated to flower-like $NiCo_2O_4$, *Anal. Chim. Acta*, 2016, **935**, 104–112.

25 A. Rehman and X. Zeng, Ionic liquids as green solvents and electrolytes for robust chemical sensor development, *Acc. Chem. Res.*, 2012, **45**, 1667–1677.

26 X. M. Li, L. F. Jiang, C. Zhou, J. P. Liu and H. B. Zeng, Integrating large specific surface area and high conductivity in hydrogenated $NiCo_2O_4$ double-shell hollow spheres to improve supercapacitors, *NPG Asia Mater.*, 2015, **7**, 165–172.

27 L. F. Shen, Q. Che, H. S. Li and X. G. Zhang, Mesoporous $NiCo_2O_4$ nanowire arrays grown on carbon textiles as binder-free flexible electrodes for energy storage, *Adv. Funct. Mater.*, 2014, **24**, 2630–2637.

28 Y. F. Zhang, M. Z. Ma, J. Yang, H. Q. Su, W. Huang and X. C. Dong, Selective synthesis of hierarchical mesoporous spinel $NiCo_2O_4$ for high-performance supercapacitors, *Nanoscale*, 2014, **6**, 4303–4308.

29 Z. Y. Yu, H. J. Li, X. M. Zhang, N. K. Liu, W. L. Tan, X. Zhang and L. L. Zhang, Facile synthesis of $NiCo_2O_4$@Polyaniline core-shell nanocomposite for sensitive determination of glucose, *Biosens. Bioelectron.*, 2016, 161–165.

30 J. Yang, M. Cho and Y. Lee, Synthesis of hierarchical $NiCo_2O_4$ hollow nanorods via sacrificial-template accelerate hydrolysis for electrochemical glucose oxidation, *Biosens. Bioelectron.*, 2016, **75**, 15–22.

31 L. Liu, H. J. Zhang, J. Yang, Y. P. Mu and Y. Wang, Self-assembled novel dandelion-like $NiCo_2O_4$ microspheres@nanomeshes with superior electrochemical performance for supercapacitors and lithium-ion batteries, *J. Mater. Chem. A*, 2015, **3**, 22393–22403.

32 X. X. Yu, Z. J. Sun, Z. P. Yan, B. Xiang, X. Liu and P. W. Du, Direct growth of porous crystalline $NiCo_2O_4$ nanowire arrays on a conductive electrode for high-performance electrocatalytic water oxidation, *J. Mater. Chem. A*, 2014, **2**, 20823–20831.

33 Z. W. Lu, L. Wu, J. J. Zhang, W. L. Dai, G. Q. Mo and J. S. Ye, Bifunctional and highly sensitive electrochemical non-enzymatic glucose and hydrogen peroxide biosensor based on $NiCo_2O_4$ nanoflowers decorated 3D nitrogen doped holey graphene hydrogel, *Mater. Sci. Eng., C*, 2019, **102**, 708–717.

34 Y. N. Qin, Y. J. Sun, Y. J. Li, C. J. Li, L. Wang and S. J. Guo, MOF derived $Co_3O_4$/N-doped carbon nanotubes hybrids as efficient catalysts for sensitive detection of $H_2O_2$ and glucose, *Chin. Chem. Lett.*, 2020, **31**, 5.

35 T. J. Liu, X. Y. Zhang, K. Fu, N. Zhou, J. P. Xiong and Z. Q. Su, Fabrication of $Co_3O_4$/$NiCo_2O_4$ nanocomposite for detection of $H_2O_2$ and dopamine, *Biosensors*, 2021, **11**, 452.

36 R. Rajendran, C. H. Zhao, R. Muniyandi, R. Krishnamoorthy, P. L. Zhu, W. L. Xuan, Z. X. Xu and F. Wang, Porous nickel oxide microsphere and $Ti_3C_2T_x$ hybrid derived from metal-organic framework for battery-type supercapacitor electrode and non-enzymatic $H_2O_2$ sensor, *Electrochim. Acta*, 2019, **322**, 134771.

37 P. P. Wang, L. Cao, Y. Chen, Y. Wu and J. W. Di, Photoelectrochemical biosensor based on $Co_3O_4$ nanoenzyme coupled with PbS quantum dots for hydrogen peroxide detection, *ACS Appl. Nano Mater.*, 2019, **2**, 2204–2211.

38 Q. Li, J. Niu, M. L. Dou, Z. P. Zhang and F. Wang, Porous microtubes of nickel-cobalt double oxides as non-enzymatic hydrogen peroxide sensors, *Chin. Chem. Lett.*, 2021, **32**, 1181–1185.

39 M. H. Wang, C. B. Wang, Y. K. Liu, B. HU, L. H. He, Y. S. Ma, Z. H. Zhang, B. B. Gui and M. Di, Nonenzymatic amperometric sensor for hydrogen peroxide released from living cancer cells based on hierarchical $NiCo_2O_4$-$CoNiO_2$ hybrids embedded in partially reduced graphene oxide, *Microchim. Acta*, 2020, **187**, 436.

40 Q. Li, W. B. Gao, X. P. Zhang, H. T. Liu, M. L. Dou, Z. P. Zhang and F. Wang, Mesoporous NiO nanosphere: a sensitive strain sensor for determination of hydrogen peroxide, *RSC Adv.*, 2018, **8**, 13401–13407.

41 X. Q. Ma, K. L. Tang, M. Y. Yang, W. B. Shi and W. X. Zhao, Metal-organic framework-derived yolk-shell hollow Ni/NiO@C microspheres for bifunctional non-enzymatic glucose and hydrogen peroxide biosensors, *J. Mater. Sci.*, 2021, **56**, 1–15.